Tissue-embedded CD4$^+$ plasticity defines mucosal immunity in Inflammatory Bowel Disease

Qinyue Jiang[1], Veerle A. Merkus[2], Ciska Lindelauf[1], Nannan Guo[3], Laura F. Ouboter[1,4], Thomas Höllt[5], Philip W. Voorneveld[4], Caroline R. Meijer-Boekel[6], Frits Koning[1], Andrea E. van der Meulen-de Jong[4], Maria Fernanda Pascutti[7], Vincent van Unen[1]

[1]Department of Immunology, Leiden University Medical Center, Leiden, the Netherlands

[2]Department of Dermatology, Leiden University Medical Center, Leiden, the Netherlands

[3]Microbiome Medicine Center, Department of Laboratory Medicine, Zhujiang Hospital, Southern Medical University, Guangzhou, China

[4]Department of Gastroenterology and Hepatology, Leiden University Medical Center, Leiden, the Netherlands

[5]Computer Graphics and Visualization, Delft University of Technology, Delft, the Netherlands

[6]Department of Pediatrics, Leiden University Medical Center, Leiden, the Netherlands

[7]Immunotherapy Center, Cancer Center Amsterdam, Amsterdam UMC location VUmc, Amsterdam, the Netherlands

Corresponding author: Vincent van Unen (v.van_unen@lumc.nl)

Address: Postzone E3-Q, P.O. Box 9600, 2300 RC Leiden, The Netherlands

Highlights:

1. IBD inflammation shapes $CD4^+$ T-cell plasticity and tissue-residency programming.
2. Correlated $CD4^+$ and cytotoxic $CD8^+$ T cells co-localize in inflamed mucosa.
3. Mucosal $CD4^+$ memory T cells show hypo-responsiveness in active IBD.
4. HLA-DR^+CD38^+ memory $CD4^+$ T cells amplify inflammation via cytokine output.

Abstract

$CD4^+$ T helper (Th) cell responses to commensal microbiota are linked to Inflammatory Bowel Disease (IBD), yet how Th programs coexist and evolve in human tissues remains poorly defined. Here, we profiled $CD4^+$ memory T cells in intestinal biopsies using immunological and histological approaches to map their phenotypes, functional states, and spatial relationships across disease states. A marked expansion of $CD4^+$ T cells concomitant with a RORγt$^+$ Th population with elevated T-bet expression was linked to progression of inflammation. Moreover, $Foxp3^+$ cells co-expressing RORγt emerged within the inflamed niche, indicating regulatory–Th17 plasticity. Trajectory visualization revealed a potential branched differentiation path towards either regulatory or tissue-resident Th17-like fates, with both termini expressing activation and proliferation markers. Correlation network analysis connected pro-inflammatory $CD4^+$ states to T-bet$^+$Granzyme-B$^+$ $CD8^+$ subsets, indicative of crosstalk between helper and cytotoxic lineages. Histology corroborated this organization, showing frequent interactions between $CD4^+$ and $CD8^+$ cells in the lamina propria and epithelial border. In functional assays, TCR stimulation during active disease revealed broad suppression of $CD4^+$ pro-inflammatory cytokines concomitant with expansion of $Foxp3^+$ cells. Conversely, HLA-DR^+CD38^+ memory subset retained multifunctionality, producing elevated levels of pro-inflammatory cytokines. Together, these results provide insight into a dynamic, tissue-embedded CD4 landscape in IBD.

Keywords

IBD; T helper cells; Plasticity; Tissue-resident cells; Mucosal immunology

Introduction

Disrupted immune responses to the gut microbiota in genetically susceptible individuals, potentially triggered by largely unknown environmental factors, contribute to the pathogenesis of Inflammatory Bowel Diseases (IBD)[1]. IBD typically follows a chronic, relapsing-remitting course, and comprises two main subtypes: Crohn's disease (CD) and ulcerative colitis (UC). UC affects the colon and is characterized by continuous mucosal lesions, whereas CD can involve any segment of the gastrointestinal tract and frequently displays transmural inflammation. Current therapeutic goals are to induce and maintain clinical, biochemical, and durable endoscopic remission to minimize bowel damage and improve long-term outcomes[2]. Neither CD nor UC has a single phenotype; both are heterogeneous with respect to clinical presentation, treatment responses, and immune profiles[3]. Management of disease remains largely reactive, with treatment adjustments commonly driven by worsening of clinical parameters. Molecular and cellular characterization that accounts for inter-individual variability in tissue pathology could better guide clinical management and advance personalized therapy in IBD[4]. Dysregulation of $CD4^+$ T cell subsets is widely implicated in chronic intestinal inflammation. In IBD, an imbalance between inflammation-promoting and immunoregulatory populations sustains mucosal damage and persistent immune activation, ultimately contributing to the development of chronic disease[5]. Upon antigen recognition, naïve $CD4^+$ T cells can differentiate into distinct effector subsets, including pro-inflammatory Th1, Th2, and Th17, as well as a regulatory T (Treg) subset[6, 7]. In the intestine, regional tissue-resident memory $CD4^+$ T cells (T_{RM}) provide long-term local immunity to microbial antigens, and can be rapidly reactivated, undergo transient proliferation, and reacquire distinct T-helper phenotypes[8]. Recent studies have highlighted that polarized T-helper cells can adopt alternative phenotypes and functionalities during disease progression, accompanied by changes in signature transcription factors and lineage-defining cytokine profiles[9, 10]. While bidirectional Treg–Th17 plasticity has been described in IBD[10, 11], the mechanisms governing this switching in human intestinal tissues across disease states remain poorly defined.

Although $CD4^+$ T cells are major contributors to chronic intestinal inflammation, the intestinal

immune landscape includes diverse cell types that interact with $CD4^+$ T cells across the lamina propria and intraepithelial compartments to shape adaptive responses in IBD. Among these, $CD8^+$ T cells, located in proximity to $CD4^+$ T cells, are thought to be implicated in epithelial injury in IBD[12, 13]. We previously identified an inflammation-associated immune network enriched for activated HLA-DR^+CD38^+ effector memory $CD4^+$ T cells in treatment-naïve IBD patients[14]. However, the phenotype, function, and trajectory of this population, particularly during disease remission, remain poorly defined.

To address these gaps, we performed immunological functional assays with spectral flow cytometry on freshly obtained intestinal biopsies and paired peripheral blood from patients with active IBD or in clinical remission, as well as non-IBD noninflamed controls. Here, we show that IBD harbors a dynamic, tissue-embedded $CD4^+$ landscape with inflammatory expansion that recedes in remission, regulatory-Th17 plasticity (Foxp3–RORγt), and branched trajectories toward regulatory and tissue-resident fates. We also show coordinated CD4–CD8 networks and a multifunctional HLA-DR^+CD38^+ memory subset that persists despite global cytokine suppression, pointing to the development of rational therapeutic strategies to rebalance resident/regulatory programs while preserving protective memory.

Results

$CD4^+$ T cells are enriched in the inflamed mucosa

To comprehensively assess intestinal and circulating T cells, together with other conventional and non-conventional lymphoid subsets, we applied a validated 37-plex full spectral flow cytometric panel[5] to single-cell suspensions of endoscopic intestinal samples (n=68) and peripheral blood mononuclear cells (PBMCs) (n=32) from 27 IBD patients (CD, n=17; UC, n=10) and 5 controls (clinical metadata listed in **Supplementary Table 1**), yielding a dataset on 3.5 million live $CD45^+$ cells (**Supplementary Fig. 1A**). Based on marker expression profiles, we delineated the intestinal T cell compartment and identified 7 major subsets: $CD4^+$ T cells, conventional $CD8\alpha\beta^+$ T cells, $CD8\alpha\alpha^+$ T cells, $CD8\alpha\beta^+$ NKT cells, double-negative (DN) T cells ($CD8\alpha^-CD8\beta^-CD4^-$), mucosal-associated invariant T (MAIT) cells, and γδ T cells (**Fig. 1A**). Next, samples were stratified by disease status (control, noninflamed, inflamed and remission),

57 disease subgroup (control, CD, UC), and intestinal location of the analyzed samples (colon and
58 ileum) (**Fig. 1B**). Cell-frequency analysis revealed pronounced heterogeneity in immune
59 composition, with $CD4^+$ T cell subsets predominating in the inflamed mucosa (**Fig. 1B**). Density
60 plots of an opt-SNE analysis highlight differential presence of the $CD4^+$ T cell subsets
61 depending on disease status (**Fig. 1C and Supplementary Fig. 1B**). Consistently, the frequency
62 of $CD4^+$ T cells was significantly increased during inflammation and decreased in remission
63 across disease types (CD, UC) and sites (colon, ileum) (**Fig. 1D**). In contrast, frequencies of
64 other major lineages declined (conventional $CD8\alpha\beta^+$ T, NKT and γδ T cells) or remained
65 unchanged ($CD8\alpha\alpha^+$ T, DN and MAIT cells) (**Supplementary Fig. 1C**) in the inflamed mucosa.

66 **Inflammation shapes the $CD4^+$ memory T cell landscape**

67 Next, we performed a t-SNE analysis of intestinal memory T cells (T_M), including the
68 $CD45RA^+CCR7^-$, $CD45RA^-CCR7^-$, and $CD45RA^-CCR7^+$ subsets gated within the $CD4^+$ population.
69 Based on the marker expression profiles, hierarchical clustering of the collective 65,732 cells
70 yielded 46 distinct T_M-helper clusters (**Fig. 2A–B and Supplementary Fig. 2A**). The associated
71 density plots display diverse distribution patterns related to disease state (**Fig. 2B**). Pearson's
72 rank correlation analysis identified four main cellular networks (**Supplementary Fig. 2B**), of
73 which two (**Fig. 2C**) correspond to the high-density regions of the noninflamed (bottom
74 clusters) and inflamed (top right clusters) groups shown in Fig. 2B, respectively. By analyzing
75 the frequencies of those clusters, we observed that CD4-15, CD4-12 and CD4-48 were
76 underrepresented during the active phase of disease (**Fig. 2D**), while CD4-13, CD4-5, CD4-7,
77 CD4-18, CD4-21 and CD4-4 were notably increased in the inflamed group and decreased
78 following the resolution of inflammation (**Fig. 2E**). The remaining clusters showed no
79 significant quantitative changes.

80 To refine the phenotypic features of subsets involved in IBD inflammation, we overlaid marker
81 expression across clusters (**Fig. 2F and Supplementary Fig. 2C**). Most $CD4^+$ T_M clusters
82 displayed $CD45RA^-CCR7^-$ effector-memory features, whereas a minority within CD4-18 and
83 CD4-21 co-expressed low levels of CCR7, consistent with a central memory phenotype
84 (**Supplementary Fig. 2C**). Compared to naïve T cells, all these $CD4^+$ T_M subsets exhibited

abundant expression of CD69, with cluster CD4-7 co-expressing CD103, indicating tissue-residency. Strikingly, the six inflammation-linked clusters (CD4-13, CD4-5, CD4-7, CD4-18, CD4-21, and CD4-4) co-expressed HLA-DR, CD38, and CD39 to varying degrees, consistent with activation. In addition, the expression of Ki-67 in CD4-5, CD4-7 and CD4-18 suggested proliferative potential. Distinct expression patterns of the transcription factors (T-bet, RORγt, Foxp3 and Helios) were observed among the $CD4^+$ T_M clusters. For example, CD4-5 and CD4-7 co-expressed RORγt and T-bet, consistent with Th1/Th17-like states, but were otherwise phenotypically similar, differing primarily by CD103 expression restricted to CD4-7. Moreover, inflammation-associated CD4-18, CD4-21 and CD4-4 expressed Foxp3, with variable RORγt and Helios, indicating Treg identity and plasticity. Furthermore, we performed PCA on frequencies of 46 $CD4^+$ T_M cell clusters (**Supplementary Fig. 2D**). Noninflamed samples (control, noninflamed IBD and remission) were clustered together and separately from inflamed samples. CD and UC samples were separated from the controls, with clear colon-ileum stratification. Overall, the inflammatory status and tissue location were the dominant source of variation.

Collectively, these findings suggest a disease-state–dependent, tissue-resident $CD4^+$ memory landscape, with heterogeneous Th1/Th17 and $Foxp3^+$ networks, whose frequencies stratify colon *versus* ileum and IBD *versus* control, increase with inflammation, and recede in remission.

Trajectory analysis reveals bifurcating inflammatory paths of $CD4^+$ memory T cell differentiation

Given the observed plasticity within $CD4^+$ T-helper subsets, we next examined how these states evolve during inflammation. We used the dynamic t-SNE visualization in Cytosplore with naïve $CD4^+$ T cells as a reference (**Fig. 3A and Supplementary Fig. 3A**)[15, 16]. Cells were initially unordered at onset of the t-SNE computation, but by stage 2 naïve cells segregated from the remaining memory cells. By stages 3–4 an interconnected network emerged with two branches bridged by cluster 13 (**Fig. 3A**). Disease-status overlays showed that the left branch comprised noninflamed clusters (CD4-12, CD4-15, CD4-48), whereas the right branch

113 contained inflammation-linked clusters (CD4-5, CD4-7, CD4-4, CD4-18, CD4-21) (**Fig. 3B**).
114 Marker expression profiles showed CD127 enrichment along the noninflamed branch and
115 uniform CD39 positivity across inflamed clusters, with concurrent increases in CD38, HLA-DR
116 and Ki-67 on the inflamed branch (**Fig. 3C**), consistent with activation and proliferation.

117 To quantify marker dynamics along putative differentiation pathways, we applied Wishbone
118 rooted at the intermediate cluster 13. This analysis revealed a clear bifurcation driven by
119 divergent expression of RORγt/CD103 *versus* Foxp3/CTLA-4/CD25/Helios (**Fig. 3D–E**),
120 delineating inflammatory trajectories toward a tissue-resident Th17-like fate (Branch I) and a
121 regulatory fate (Branch II), respectively. Activation markers (HLA-DR, CD38, CD39, Ki-67) rose
122 along the inflamed branch, supporting a model of inflammation-associated maturation from
123 a shared intermediate. Additional overlays further corroborated branch identity (**Fig. 3C–E**):
124 CD161 and CCR6, canonical Th17 features, were concentrated along the inflamed, tissue-
125 resident branch (Branch I), whereas CCR4 and CD27, characteristic of Treg/less-differentiated
126 memory, were biased toward the inflamed, regulatory branch (Branch II). CXCR3 aligned with
127 T-bet–associated segments within Branch I, CD69 was broadly elevated across both branches,
128 and a small $CD56^+$ subset localized in the noninflamed branch, suggesting NK-like attributes.

129 Taken together, these analyses reveal a bifurcation from a shared intermediate into two
130 inflammatory trajectories, one toward a tissue-resident Th17-like effector state and the other
131 toward a regulatory fate, signifying inflammation-driven diversification of $CD4^+$ T-helper
132 memory programs.

133 **Coordination of $CD4^+$ and $CD8^+$ T-cell programs at the mucosal interface in IBD**

134 To interrogate potential CD4–CD8 crosstalk in the intestine, we next characterized the $CD8^+$ T-
135 cell compartment. Unsupervised dimensionality reduction identified 20 phenotypically
136 distinct $CD8^+$ clusters (**Supplementary Fig. 4A**). We then integrated these $CD8^+$ clusters with
137 the $CD4^+$ memory clusters and performed a Pearson correlation network analysis, resolving
138 five multi-lineage cellular networks (**Fig. 4A**), characterized by strong within-network positive
139 correlations and between-network anticorrelations. Network 3 contained the five
140 inflammation-associated $CD4^+$ clusters (CD4-4, CD4-5, CD4-7, CD4-18, CD4-21) together with

141 five $CD8^+$ clusters (CD8-2, CD8-3, CD8-8, CD8-9, CD8-10). Four of the five $CD8^+$ clusters
142 displayed a $CCR7^-CD45RO^+CD45RA^-$ effector-memory phenotype, whereas CD8-3 was
143 $CCR7^-CD45RO^-CD45RA^+$, consistent with a terminally differentiated (T_{EMRA}-like) state (**Fig. 4B**
144 **and Supplementary Fig. 4B**). CD8-3, CD8-8, and CD8-9 showed a conventional CD8αβ
145 phenotype; clusters 8 and 9 expressed Granzyme-B, indicating cytolytic potential, and CD8-9
146 additionally expressed CD103, consistent with tissue residency. In contrast, CD8-2 and CD8-10
147 lacked CD8β and co-expressed CD4 with CD8α, alongside RORγt and T-bet (**Fig. 4C and**
148 **Supplementary Fig. 4B**). Notably, all five $CD8^+$ clusters were significantly increased, or trended
149 upward, in inflamed samples in parallel with their correlated $CD4^+$ memory clusters (**Fig. 4D**).
150 Conversely, four $CD8^+$ clusters were reduced in inflammation (**Supplementary Fig. 4C**),
151 indicating contraction of noninflamed/homeostatic states outside Network 3.

152 To define the spatial organization of resident $CD4^+$ and $CD8^+$ T cells in the inflammatory
153 microenvironment, we performed six-color multispectral immunofluorescence on inflamed
154 colonic tissue from patients with CD (n=2) and UC (n=3), as well as on noninflamed colonic
155 tissue from healthy donors (n=2), displaying four representative regions of interest (ROIs) per
156 group. We simultaneously detected E-cadherin, CD3, CD4, CD8, CD103, and DAPI (**Fig. 4E**).
157 Compared with controls, IBD samples showed increased T-cell infiltration within the lamina
158 propria and along the epithelial interface, with frequent juxtaposition of $CD4^+$ and $CD8^+$ cells
159 (white arrows). $CD103^+$ intraepithelial cells were predominantly $CD8^+$ (yellow arrows),
160 whereas $CD103^+CD4^+$ cells localized near the epithelial border or within the lamina propria
161 (magenta arrows), consistent with coordinated resident programs at the mucosal interface.
162 Notably, this spatial pattern accords with the trajectory analysis (**Fig. 3**), which revealed
163 progressive CD103 induction along the inflammatory $CD4^+$ branch, linking phenotypic
164 residency programming to tissue positioning.

165 **Inflammation dampens TCR-mediated activation of $CD4^+$ memory T cells**

166 To assess $CD4^+$ T cell function, we stimulated single-cell suspensions from intestinal biopsies
167 with α-CD3/α-CD28 for 6 hours and profiled CD40L together with cytokines characteristic of
168 Th1 (IL-2, TNFα, IFNγ), Th2 (IL-13, IL-4), Th17 (IL-17A, IL-21, IL-22), and Treg (IL-10) by spectral

169 flow cytometry (**Supplementary Fig. 5A**). Data from noninflamed samples (controls,
170 noninflamed IBD, remission) were pooled and compared with inflamed samples. Two
171 experimental batches showed concordant trends and are presented separately in
172 Supplementary Fig. 5B–C, and the combined cohort is shown in Figure 5.

173 CD40L was robustly induced by stimulation in all groups but rose less in inflamed tissue,
174 indicating attenuated activation (**Fig. 5A**). HLA-DR$^+$CD38$^+$ CD4$^+$ T_M cells were higher at baseline
175 in inflamed mucosa and remained at similar frequencies after stimulation (**Fig. 5B**). Although
176 CXCL13$^+$CD4$^+$ T_M cells, indicative of a T follicular helper-like subset, were also increased at
177 baseline in inflamed tissue, their frequencies were instead reduced after stimulation
178 compared with noninflamed samples (**Fig. 5C**).

179 We next quantified cytokine production within the memory compartment (**Fig. 5D–E and**
180 **Supplementary Fig. 5C**). After 6 hours, Th1 cytokines (IL-2, TNFα, IFNγ) predominated, Th17
181 cytokines (IL-17A, IL-21, IL-22) were lower in abundance, and Th2/Treg cytokines (IL-13, IL-4,
182 IL-10) were largely rare. Moreover, TNFα was significantly decreased in the inflamed group,
183 with IL-2 and IFNγ showing only mild reductions (**Fig. 5D**); these differences persisted when
184 gating on activated CD40L$^+$ cells (**Fig. 5E**). IL-17A and IL-21 were largely unchanged, while IL-
185 22 trended lower (**Supplementary Fig. 5C**). IL-13/IL-4 showed a small but statistically
186 significant difference with low absolute frequencies, and IL-10 showed no clear change (**Fig.**
187 **5D**). In the CD8$^+$ memory compartment, CD40L expression did not change after stimulation,
188 but IL-2 production was significantly reduced in inflamed versus noninflamed tissue, whereas
189 TNFα, IFNγ and IL-17A were comparable (**Supplementary Fig. 6A-B**).

190 To investigate mechanisms of reduced cytokine production, we related Foxp3$^-$ effector output
191 to Foxp3$^+$ Treg abundance. Significant negative correlations with Foxp3$^+$ frequency were
192 observed for IFNγ and IL-17A, with a trend for TNFα (**Fig. 5F**). Th2 cytokines and IL-10 were
193 not significantly correlated. In addition, a multifunctional subset co-producing IL-2, TNFα and
194 IFNγ was likewise diminished in inflamed tissue upon stimulation and inversely associated
195 with Foxp3$^+$ frequency (**Fig. 5G–H**).

196 Applying the same stimulation to paired blood samples revealed comparable CD40L induction

197 and cytokine production between inflamed and noninflamed groups (**Supplementary Fig. 6C-**
198 **E**), suggesting that the hypo-responsiveness is localized to the tissue.

199 Collectively, despite intact proximal activation through TCR engagement, $CD4^+$ T_M cells from
200 inflamed mucosa display selectively blunted Th1 effector function and reduced
201 multifunctionality, features that are tissue-localized and in part linked to increased regulatory
202 burden.

203 **HLA-DR^+CD38^+ memory $CD4^+$ T cells in IBD are tissue-resident, proliferative, and**
204 **multifunctional**

205 We previously noted an expansion of activated HLA-DR^+CD38^+ effector-memory $CD4^+$ T cells
206 in treatment-naïve IBD[14]. Here, including both active disease and remission, we confirmed
207 that HLA-DR and CD38 were upregulated across central memory (T_{CM}), effector memory (T_{EM})
208 and terminally differentiated effector memory (T_{EMRA}) subsets (**Fig. 6A**), and that the HLA-
209 DR^+CD38^+ fraction was increased in inflamed tissue and reduced in remission (**Fig. 6B**).

210 Analysis of the transcription factor composition demonstrates that within HLA-DR^+CD38^+
211 memory cells, a large subset (~25%) was negative for the lineage factors T-bet, RORγt and
212 Foxp3, with single-positive $Foxp3^+$ cells comprising a minority (~10%) (**Fig. 6C**). Nonetheless,
213 RORγt expression was clearly enriched (~23%) and included a subset co-expressing T-bet
214 (~20%). Cells co-expressing Foxp3 and Helios, markers linked to Treg stability, were present at
215 lower but increased levels in HLA-DR^+CD38^+ cells compared with HLA-DR^-CD38^- cells
216 (**Supplementary Fig. 7A–C**), indicating a small embedded regulatory-like subset.

217 Next, we compared the phenotypic profiles among HLA-DR/CD38-defined memory subsets
218 within inflamed tissue. Compared with HLA-DR^-CD38^- memory cells, the HLA-DR^+CD38^+
219 population showed higher CD25 and lower CD127 (**Fig. 6D**), indicating enhanced IL-2 receptor
220 signaling and recent activation. They also upregulated CTLA-4 and CD39 (**Fig. 6E**), consistent
221 with engagement of regulatory pathways and ectonucleotidase activity that can generate
222 immunomodulatory adenosine. The same cells expressed increased CD103 and CD69 (**Fig. 6F**),
223 markers of tissue residency and epithelial retention, and exhibited elevated Ki-67 (**Fig. 6G**),
224 indicating ongoing proliferation. T-bet and RORγt were enriched in the HLA-DR^+CD38^+ subset

225 (**Fig. 6H**), supporting polarization toward Th1/Th17 programs. Cells single-positive for HLA-DR
226 or CD38 generally displayed intermediate levels across these features (**Fig. 6D–H**), placing
227 them between quiescent double-negative and fully activated double-positive states.

228 Finally, we assessed cytokine production by HLA-DR$^+$CD38$^+$ CD4$^+$ T_M cells. Upon stimulation
229 with α-CD3/α-CD28, this subset produced more IFNγ, IL-21, IL-22, IL-10 than in HLA-DR$^-$CD38$^-$
230 counterparts (**Fig. 6I**). In contrast, IL-2, TNFα, IL-17A and Th2 cytokines (IL-13/IL-4) were
231 comparable between groups (**Fig. 6I**), pointing to selective multifunctionality. t-SNE
232 visualization of cytokine expression within the HLA-DR$^+$CD38$^+$ compartment (**Supplementary**
233 **Fig. 7)** showed that activated Th1, Th17, Tfh/Th22-like cells largely occupied distinct regions
234 with only limited overlap; within this landscape, polyfunctional IFNγ$^+$IL-2$^+$TNFα$^+$ Th1-type cells
235 predominated, while IL-17A was mainly produced by separate cells, with only a small subset
236 co-expressing IL-17A together with these Th1 cytokines. Taken together with their activation,
237 residency, and proliferative features, these data position HLA-DR$^+$CD38$^+$ CD4$^+$ T_M cells as
238 tissue-embedded effectors that can both amplify inflammation and modulate it through
239 targeted cytokine programs.

240 **Discussion**

241 Our findings show that inflammation in IBD reshapes the intestinal T cell landscape, marked
242 by an expansion of activated CD4$^+$ memory T cells and contraction of other T cell subsets.
243 These CD4$^+$ memory T cells displayed a tissue-resident, proliferative phenotype and correlated
244 with specific cytotoxic CD8$^+$ T cell subsets, suggesting coordinated mucosal immune responses.
245 Their numbers declined in remission, underscoring inflammation-dependent expansion. We
246 found these cells to be functionally hyporesponsive upon TCR stimulation, producing reduced
247 TNFα and IFNγ and displaying limited polyfunctionality. This functional restraint was inversely
248 correlated with local Foxp3$^+$ Treg abundance. However, a specific CD4$^+$ memory T cell subset
249 expressing HLA-DR and CD38 maintained polyfunctionality in inflamed IBD. In essence, active
250 IBD lesions are characterized by the coexistence of a broadly hyporesponsive CD4$^+$ memory
251 pool and a smaller HLA-DR$^+$CD38$^+$ subset that remains highly multifunctional, suggesting
252 differential regulation within the wider CD4$^+$ compartment under chronic inflammatory

253 conditions.

254 Our high-dimensional approach also captured several 'unconventional' T-cell subsets (γδ T
255 cells, MAIT cells and NKT-like cells)[17, 18]. We noted that γδ T cells, which normally reside
256 abundantly in intestinal epithelium, were markedly decreased in the inflamed mucosa in our
257 IBD cohort. This aligns with reports that mucosal γδ T cells are perturbed in IBD, although
258 findings have varied[19]. Similarly, invariant NKT cells (CD1d-restricted T cells) were diminished
259 in our inflamed samples. Consistently, clinical studies have reported that type 1 NKT cells are
260 reduced in the blood and intestine of CD and UC patients, whereas type 2 NKT cells can
261 accumulate in UC lamina propria, potentially contributing to typical Th2 responses[20]. MAIT
262 cells typically accumulate in the gut and help regulate responses to microbiota[21-23]; however,
263 we did not observe significant changes in their frequency in our dataset, in contrast to
264 previous studies. Nonetheless, our observations reinforce the idea that intestinal
265 inflammation can differentially affect innate-like T-cell populations.

266 A central finding of our study is the plasticity of $CD4^+$ T-helper cells under inflammatory
267 conditions. We identified $ROR\gamma t^+$ Th17-lineage subsets with divergence into Th1-like (T-
268 $bet^+IFN\gamma^+$) or Treg-like ($Foxp3^+CTLA\text{-}4^+$) fates, indicating context-dependent bifurcation within
269 the IBD mucosa. In our cohort, mixed Th1/Th17 subsets (clusters CD4-13, CD4-5, and CD4-7)
270 were selectively expanded in patients with active disease and returned toward baseline
271 frequencies in patients in remission, directly linking these plastic states to clinical
272 inflammation. This supports the concept that Th17 cells are highly flexible, adopting pro- or
273 anti-inflammatory phenotypes depending on the local cytokine milieu[24, 25]. In line with this,
274 $HLA\text{-}DR^+CD38^+$ EM $CD4^+$ T cells, previously also identified as a central disease-associated
275 population in treatment-naïve IBD[14] and as activated Th1/Th17 cells in CD-associated perianal
276 fistulas[26], likely represent a clinically relevant manifestation of this plastic Th17/Th1
277 continuum. Some studies have shown that IL-23 promotes the emergence of pathogenic Th17
278 cells that gain IFNγ-producing, Th1-like features, including $IL\text{-}17A^+IFN\gamma^+$ and ex-Th17 effectors,
279 particularly in T cell–transfer colitis models[27-29]. Blocking IL-23 in these models attenuates
280 these pathogenic populations and ameliorates colitis, and, in patients, antibodies targeting IL-
281 12/23p40 or IL-23p19 induce and maintain remission in both CD and UC[30-33]. Moreover,

282 Heredia *et al.* demonstrated that IL-12 can drive gut-homing TIGIT^{-}CD38^{+} memory T cells
283 towards an ex-Th17/Th1-like pathogenic phenotype in a subset of pediatric CD with a severe
284 disease course[34]. In contrast, IL-17 neutralization failed to show efficacy in IBD and in some
285 trials was associated with worsening disease and paradoxical intestinal inflammation, likely
286 due to its role in mucosal integrity. These findings underscore the need to recalibrate, not
287 eliminate, Th17 responses.

288 Our trajectory analysis further supports a model in which Th17-like cells can shift toward
289 Foxp3^{+} regulatory phenotypes in response to inflammation. We observed RORγt^{+}Foxp3^{+}
290 double-positive cells enriched in inflamed tissue, potentially representing Th17-derived Tregs.
291 Expression of Foxp3 in RORγt^{+} cells may in part reflect activation rather than bona fide
292 regulatory function; however, these cells also upregulated CD39 and CTLA-4, consistent with
293 a Treg-like program potentially adapted to suppress Th17-skewed responses. Previous studies
294 similarly suggest that Tregs are also plastic and can transiently adopt lineage-defining
295 transcription factors to better control specific effector responses[35-37]. Interestingly, we noticed
296 these cells simultaneously expressing CD161, though it is typically linked to a RORγt-driven
297 transcriptional program and denotes a pro-inflammatory fate. This observation is consistent
298 with previous findings that reported existence of CD161^{+} regulatory T cells with preserved
299 suppressive capacity[38]. Conversely, Foxp3^{+} Tregs may become unstable under inflammatory
300 pressure[39], losing Foxp3 and acquiring effector functions. In support of this, single-cell
301 profiling of ileal CD4^{+} T cells in CD identified proinflammatory FOXP3^{+} Treg subsets with TNFα-
302 driven gene programs, impaired suppressive function, and enhanced cytokine production[40].
303 Thus, bidirectional plasticity between Th17 and Treg lineages may dynamically tune
304 inflammation and resolution. Therapeutically, this suggests restoring the Th17/Treg balance
305 as an attractive target. Low-dose IL-2, which preferentially expands Tregs, has shown safety
306 and partial efficacy in UC[41], though Treg instability remains a concern. Combining Treg-
307 expanding strategies with cytokine blockade (e.g., IL-6/STAT3 inhibition) or next-generation
308 antigen-specific or CAR-engineered Tregs may improve durability[39, 42, 43].

309 Our data also highlight that clusters on the Th17-like inflammatory trajectory upregulated
310 CD69 and CD103, indicating a transition to tissue-resident memory T cells. Tissue-resident T

311 cells reside in the gut mucosa for decades[44], where they can react swiftly to local stimuli[45]. In
312 line with this, $CD4^+$ T_{RM} have been shown to be expanded and to constitute a major TNFα-
313 producing population in active CD[46], supporting their pathogenic potential. Recent work in CD
314 identified pathogenic $CD103^+CD161^+CCR5^+$ $CD4^+$ T cells with innate-like IFNγ responses and
315 epithelial localization[47]. These cells exhibited innate-like effector functions, produced large
316 amounts of IFNγ upon stimulation, and clustered near the epithelium. We similarly observed
317 inflammation-linked $CD4^+$ tissue-resident memory cells (exemplified by cluster 7), which likely
318 represent the long-lived pathogenic effectors that embed in the gut tissue and could drive
319 disease recurrence or persistence. The presence of such inflammation-prone resident
320 memory T cells might explain why some patients relapse quickly after treatment withdrawal.

321 Correlation network analysis of our data demonstrated that the inflammation-associated
322 $CD4^+$ clusters were tightly linked to certain $CD8^+$ T-cell clusters (forming a multi-lineage
323 network). These CD8 subsets, which expanded in active disease, included $CD8\alpha\beta^+$ cytotoxic
324 tissue-resident T cells and unconventional $CD4^+CD8\alpha^+CD8\beta^-$ tissue-resident T cells, previously
325 described by Lockhart et al[48], co-expressing T-bet and RORγt in our data. Moreover, our
326 findings are consistent with reports that ileal $CD8^+$ tissue-resident memory T cells acquire
327 context-dependent inflammatory programs in IBD[49]. Jaeger *et al.* further reported a spatial
328 redistribution of $CD8^+$ T cells in CD, with a loss of $CD8^+$ IELs and a concomitant increase in
329 $CD103^+$ resident cells within inflamed tissue, suggesting that the depletion of $CD8^+$ IELs may
330 weaken epithelial barrier defense, while their accumulation in the lamina propria, together
331 with $CD4^+$ T cells, could amplify inflammation[50]. Spatially, multiplex immunofluorescence
332 revealed dense aggregates of $CD4^+$ and $CD8^+$ T cells intermingled in inflamed IBD tissues. $CD8^+$
333 T cells (especially $CD8\alpha\beta^+CD103^+$ IELs) were observed within or just below the epithelium,
334 often adjacent to $CD4^+$ cells, pointing to possible crosstalk. This coordinated localization
335 suggests a scenario where $CD4^+$ T cells and $CD8^+$ cytotoxic T cells jointly contribute to
336 epithelial injury in IBD.

337 Our study has limitations that open avenues for further research. Our data are cross-sectional;
338 longitudinal sampling before, during, and after therapy would be valuable to observe T-cell
339 state transitions and confirm which changes are causes or consequences of healing. Technical

340 aspects like the use of *ex vivo* stimulation should be expanded with antigen-specific
341 stimulation assays to mimic chronic exposure to microbial antigens. The duration of T-cell
342 activation should be extended to elicit a broader range of cytokines, and provide clearer
343 evidence of functional exhaustion. Finally, it would be intriguing to molecularly characterize
344 the epigenetic landscape of these inflammation-adapted T cells.

345 In summary, this study provides an integrated view of how inflammation sculpts the intestinal
346 T-cell landscape in IBD, revealing distinct T-cell states linked to disease activity. We propose
347 that IBD flares are driven by a network of tissue-resident, Th17/Th1-skewed $CD4^+$ memory T
348 cells and cytotoxic $CD8^+$ T cells positioned at the mucosal interface, whose pathogenic activity
349 is counterbalanced by an expanding regulatory T-cell compartment. When inflammation
350 subsides (either naturally or via treatment), this pathogenic network contracts and the
351 regulatory arm regains dominance, restoring immune homeostasis. These findings underscore
352 the plasticity of mucosal T cells in inflammation, likely shaping patient-specific outcomes.
353 Targeting pathogenic T-cell memory while reinforcing regulatory circuits may offer a path to
354 durable IBD remission, offering opportunities for the development of more targeted
355 therapeutics.

356 **Materials and Methods**

357 Patients

358 IBD patients (minimum age 12 years old) were recruited from the Department of
359 Gastroenterology and the pediatric department at Leiden University Medical Center (LUMC).
360 Patients either had a prior diagnosis of IBD or underwent diagnostic ileocolonoscopy based
361 on clinical suspicion of new-onset IBD. Controls were patients $\geq$ 18 years old known with
362 another disease, such as history of colorectal cancer or familial colon cancer, who underwent
363 a surveillance ileocolonoscopy. The studies were reviewed and approved by the Medical
364 Ethical Committee of LUMC. After informed consent, fresh biopsies and peripheral blood were
365 obtained directly at the endoscopy room according to protocol P15.193. Fresh samples were
366 processed (see below) and results were stored in the LUMC-IBD biobank (protocol RP25.075).

367 The phenotype characterization cohort included 68 intestinal samples from 27 patients (CD,

368 n=17; UC, n=10) and controls (n=5). T cell receptor stimulation assays were conducted with
369 two cohorts of patients. The first included 20 intestinal samples from 6 IBD patients (CD, n=3;
370 UC, n=3), and 3 controls, while the second included 25 intestinal samples from 10 patients
371 (CD, n=5; UC, n=5) and 4 controls. Samples from 3 of these controls and 7 of these patients
372 (CD, n=3; UC, n=4) were utilized for phenotypical characterization as well.

373 Sample and clinical data collection

374 The clinical characteristics of all patients are shown in Supplementary Table 1. Samples from
375 rectum, colon and ileum, both from inflamed and endoscopic noninflamed mucosa (if
376 available) were collected from IBD patients. Noninflamed mucosa were bowel segments never
377 inflamed or bowel segments currently in endoscopic remission (previously involved segment).
378 Peripheral blood was drawn from all participants at the time of endoscopy.

379 Patients were classified according to the Montreal classification regarding age at diagnosis,
380 location/extent of disease and behavior. In CD patients, the inflamed segment of each patient
381 was classified according to the SES-CD, as inactive (0-2), mild (3-6), or moderate-severe (≥7).
382 In UC patients, severity of disease was scored according to the endoscopic Mayo score, as
383 inactive (0), mild (1) or moderate-severe (2-3).

384 Isolation of single cells from endoscopic intestine and peripheral blood

385 Single-cell suspensions were prepared from fresh endoscopic biopsies as previously
386 described[5]. Briefly, tissue samples were collected in Hank's balanced salt solution (HBSS,
387 ThermoFisher) and treated with 1 mM ethylenediaminetetraacetic acid (EDTA, J. T. Baker)
388 under rotation for 2 × 45 minutes at 37°C to separate the epithelium from the lamina propria
389 and release the intraepithelial lymphocytes. To obtain single cells from the lamina propria,
390 biopsies were subsequently washed with HBSS and incubated with 5 mL Iscove's Modified
391 Dulbecco's Media (IMDM) (Lonza) containing 2% Fetal Calf Serum (FCS) (Bodinco), 1,000U/mL
392 collagenase IV (Worthington), and 10 mg/mL DNase I grade II (Roche Diagnostics) for 1.5 hours
393 at 37°C. Cells isolated from both the epithelium and lamina propria were then pooled and
394 filtered through a 70 µm cell strainer and collected by centrifugation. To remove dead cells,
395 the cell pellets were incubated with 10 mg/mL DNase I in 5 ml 2% FCS/IMDM and filtered

396 through a 30 µm cell strainer. The single-cell suspensions were collected after centrifugation
397 and resuspended in IMDM complete medium supplemented with 2 mM L-glutamine (Lonza),
398 10% human serum, 100 U/mL Penicillin-Streptomycin (ThermoFisher), 0.25 ug/ml
399 Amphotericin B (Gibco), 100 µg/mL Normocin (InvivoGen) at 4°C for future steps.

400 PBMCs were isolated from freshly drawn heparin anticoagulated blood samples using Ficoll-
401 Paque™ density-gradient centrifugation. Isolated cells were washed with phosphate-buffered
402 saline (PBS), counted, and 1 million cells were stored in 20% FCS/RPMI at 4°C for future steps.

403 T-cell activation assay

404 Non-tissue culture-treated plates were incubated with 4 µg/mL goat anti-mouse IgG (Jackson
405 ImmunoResearch) at 4°C overnight in PBS and subsequently with 2.5 µg/mL α-CD3 (clone
406 Hit3a, ThermoFisher) at 37 °C for 3 hours in PBS. The fresh intestinal single cells and PBMCs
407 were seeded in the α-CD3 pre-coated plates with 1 µg/mL α-CD28 (clone CD28.2,
408 ThermoFisher) in complete medium for 6 h at 37 °C. In cohort 1, brefeldin A (1:1000, Sigma-
409 Aldrich) was added for the final 5 hours; in cohort 2, monensin (1:1500, BD GolgiStop™) was
410 added for the final 3 h. Monensin and brefeldin A were used in separate settings but yielded
411 comparable cytokine retention efficiency. Data from both experiments were therefore
412 combined.

413 Full-spectrum flow cytometry

414 For surface staining, cells were incubated with fluorochrome-conjugated antibodies, human
415 Fc block and monocyte block (BioLegend) for 30 min at 4 °C in 0.5% FCS/PBS. Cells were then
416 fixed/permeabilized using Foxp3/Transcription Factor Staining Buffer Set (ThermoFisher).
417 Subsequently, intracellular staining for transcription factors, cytokines and Ki67 was
418 performed for 45 min at 4 °C in Perm Wash Buffer (ThermoFisher). Samples were measured
419 on 5-laser Aurora (Cytek), and unmixed with single stained controls on PBMCs or UltraComp
420 eBeads (ThermoFisher) on the SpectroFlo platform (Cytek). Unstained reference controls used
421 to subtract autofluorescence were paired to their corresponding fully stained samples. Sample
422 processing, staining and measurement for phenotypic identification were performed within
423 the same day; cells for cytokine profile identification were fixed and stored at 4 °C in 0.5%

424 FCS/PBS overnight, subsequently stained with intracellular antibodies and measured the
425 following day. To account for technical variation, reference samples of PBMCs and tonsillar
426 mononuclear cells from single donors were included in every spectral cytometry experiment.
427 Data were analyzed with FlowJo software version 10 (Tree Star Inc) and OMIQ online platform
428 (https://www.omiq.ai/, Inc., Santa Clara, CA, USA). All antibodies used are listed in
429 Supplementary Table 2 and 3.

430 Multispectral immunofluorescence and microscopy

431 Freshly obtained biopsies were formalin-fixed and paraffin-embedded by the Department of
432 Pathology at LUMC. 4 µm sections were cut using a microtome, mounted on silane-coated
433 slides, and dried overnight at 37 °C. Sections were deparaffinized using three rounds of xylene,
434 followed by three 100% ethanol washes, blocking of endogenous peroxidase for 20 min, and
435 then rinsed with 70% and 50% ethonal and Milli-Q water. For antigen retrieval, sections were
436 boiled in 1x Tris-EDTA buffer (10 mM, pH 9) for 10 min and allowed to cool down for ± 60 min.
437 Sections were stained in the dark in 5 staining cycles. Each staining cycle had the following
438 procedure: All sections were blocked by Superblock (Thermofisher) for 10 min at room
439 temperature (RT). Excess superblock was removed, and slides were incubated with primary
440 antibody for 1hr at RT. After incubation, tyramide signal amplification was performed with
441 poly-HRP (immunologic) for 10 min at RT, followed by incubation with Opal (Akoya Biosciences)
442 for 10 min in the dark at RT according to manufacturer's protocol. Next, sections were boiled
443 in 1x citrate buffer (10 mM, pH 6) for 15 min to permit further staining cycles. The primary
444 staining sequence followed the order of CD3, E-cadherin, CD103, CD8 and CD4 (antibodies
445 used are listed in Supplementary Table 4). The opal staining sequence followed the order of
446 520, 690, 620, 650 and 570. Lastly, the sections were incubated with 1 µM DAPI for 15 min at
447 RT for nuclear counterstaining, and mounted using ProLong Gold Antifade Reagent (CAT#9071,
448 CST). Each ROI was imaged at 20× magnification with the Vectra 3.0 Automated Quantitative
449 Pathology Imaging System (Perkin Elmer). Inform software (Akoya) was used for spectral
450 separation of Opals. Qupath software (version 0.6.0) was further used for image analysis.

451 Data analysis

452 Dimensionality reduction (opt-SNE) on $CD3^+$ T cell data was performed on OMIQ following the
453 R package "PeacoQC" to perform automated cleaning of anomalies and arcsinh-
454 transformation. Subsequently, pre-processed $CD4^+$ memory T cells and $CD8\alpha^+$ T cells were
455 exported and analyzed by t-SNE (each downsampled to 1,000 cells for visualizations) in
456 Cytosplore version 2.3.1[16]. The t-SNE computation dynamics to predict the trajectory of CD4
457 memory T cells was performed by Cytosplore, as demonstrated in our previous work[15].
458 Wishbone analysis of IBD-associated clusters was conducted in OMIQ, with CD4-13 cluster as
459 starting point. PCA of the samples for cell cluster frequencies was performed using the R-
460 package 'pca3d', where the centroid for each patient group is plotted in a scatter plot. The R
461 package 'corrplot' was used to calculate the correlation networks of cell frequencies of the
462 identified cell subsets.

463 Statistics

464 Data were presented as median and interquartile range. Patient group comparisons were
465 performed using two-tailed Kruskal–Wallis test followed by Dunn's test for multiple
466 comparisons. Cytokine proportions between the noninflamed and inflamed groups (Fig. 5D, E,
467 and G) were analyzed using two-tailed Mann–Whitney tests, while comparisons between the
468 HLA-DR^-CD38^- and HLA-DR^+CD38^+ populations (Fig. 6I) were performed using Wilcoxon tests
469 (GraphPad Prism version 10.2.3). Linear Mixed-effects model implemented in R was used to
470 account for stimulation effects within each inflammation group (Fig. 5A–C).

471 Data availability

472 Data will be made publicly available on Flow Repository upon publication of the manuscript.

473 **Acknowledgments**

474 We thank all the patients for participating in this study. We thank all gastroenterologists and
475 nurses for performing endoscopies and obtaining patient materials. We thank Zhixian Wang,
476 Yizhi Wang, Yanling Xiao, Oscar R. J. van Hengel, Zheng Li and Noel F. de Miranda for valuable
477 contributions to experimental setting and data analysis. In addition, we thank groupmates for
478 insightful discussions and assistance with experiments, and all the operators in the Flow

Cytometry Core Facility of the LUMC for their technical assistance during measurements on Cytek Aurora.

Author contributions

QJ, FK, MFP, AM and VvU conceived the study and wrote the manuscript. AvdM-dJ, CRM-B, PV and LFO offered clinical advice and assisted in biopsies collection. QJ performed the experiments and analyzed the data. NG analyzed part of PBMC data. VAM helped to perform the staining of tissue sections, TH provided conceptual input for trajectory analysis, and CL helped to perform the isolation of single cells.

Funding information

This research was supported by Leiden University Medical Center (QJ, VAM, CL, LFO, CRM-B, PV, FK, AvdM-dJ, MFP, VvU). QJ was supported by ImmuneHealthSeed (Powered by Health-Holland, Top Sector Life Sciences & Health) and China Scholarship Council (202006160039), VvU was supported by HORIZON-MSCA-PF (101109788), MFP and FK were supported by the collaboration project TIMID (LSHM18057-SGF) financed by the PPP allowance made available by Health-Holland, Top Sector Life Sciences & Health to Samenwerkende Gezondheidsfondsen (SGF) to stimulate public-private partnerships and co-financing by health foundations that are part of the SGF. NG was supported by the National Natural Science Foundation of China (82302608) and the Guangdong Basic and Applied Basic Research Foundation (SL2025A04J3774).

Conflict of interest statement

The authors declare that the research was conducted in the absence of any commercial or financial relationships that could be construed as a potential conflict of interest.

Reference

1. de Souza HS, Fiocchi C. Immunopathogenesis of IBD: current state of the art. *Nat Rev Gastroenterol Hepatol* 2016; **13**(1)**:** 13–27.

2. Turner D, Ricciuto A, Lewis A, D'Amico F, Dhaliwal J, Griffiths AM *et al.* STRIDE-II: An Update on the Selecting Therapeutic Targets in Inflammatory Bowel Disease (STRIDE)

Initiative of the International Organization for the Study of IBD (IOIBD): Determining Therapeutic Goals for Treat-to-Target strategies in IBD. *Gastroenterology* 2021; **160**(5)**:** 1570–1583.

3. Maaser C, Sturm A, Vavricka SR, Kucharzik T, Fiorino G, Annese V *et al.* ECCO-ESGAR Guideline for Diagnostic Assessment in IBD Part 1: Initial diagnosis, monitoring of known IBD, detection of complications. *J Crohns Colitis* 2019; **13**(2)**:** 144–164.

4. Atreya R, Neurath MF. Biomarkers for Personalizing IBD Therapy: The Quest Continues. *Clin Gastroenterol Hepatol* 2024; **22**(7)**:** 1353–1364.

5. Maloy KJ, Powrie F. Intestinal homeostasis and its breakdown in inflammatory bowel disease. *Nature* 2011; **474**(7351)**:** 298–306.

6. Ma Z, Wang Z, Cao J, Dong Y, Chen Y. Regulatory roles of intestinal CD4(+) T cells in inflammation and their modulation by the intestinal microbiota. *Gut Microbes* 2025; **17**(1)**:** 2560019.

7. Shale M, Schiering C, Powrie F. CD4(+) T-cell subsets in intestinal inflammation. *Immunol Rev* 2013; **252**(1)**:** 164–182.

8. Sheridan BS, Lefrancois L. Regional and mucosal memory T cells. *Nat Immunol* 2011; **12**(6)**:** 485–491.

9. Saravia J, Chapman NM, Chi H. Helper T cell differentiation. *Cellular & Molecular Immunology* 2019; **16**(7)**:** 634–643.

10. DuPage M, Bluestone JA. Harnessing the plasticity of CD4(+) T cells to treat immune-mediated disease. *Nat Rev Immunol* 2016; **16**(3)**:** 149–163.

11. Wang L, Liang Y, Zhao C, Ma P, Zeng S, Ju D *et al.* Regulatory T cells in homeostasis and disease: molecular mechanisms and therapeutic potential. *Signal Transduct Target Ther* 2025; **10**(1)**:** 345.

12. Casalegno Garduno R, Dabritz J. New Insights on CD8(+) T Cells in Inflammatory Bowel Disease and Therapeutic Approaches. *Front Immunol* 2021; **12:** 738762.

13. Corridoni D, Antanaviciute A, Gupta T, Fawkner-Corbett D, Aulicino A, Jagielowicz M *et al.* Single-cell atlas of colonic CD8(+) T cells in ulcerative colitis. *Nat Med* 2020; **26**(9)**:**

1480–1490.

14. van Unen V, Ouboter LF, Li N, Schreurs M, Abdelaal T, Kooy-Winkelaar Y *et al.* Identification of a Disease-Associated Network of Intestinal Immune Cells in Treatment-Naive Inflammatory Bowel Disease. *Front Immunol* 2022; **13:** 893803.

15. Li N, van Unen V, Hollt T, Thompson A, van Bergen J, Pezzotti N *et al.* Mass cytometry reveals innate lymphoid cell differentiation pathways in the human fetal intestine. *J Exp Med* 2018; **215**(5)**:** 1383–1396.

16. Höllt T, Pezzotti N, van Unen V, Koning F, Eisemann E, Lelieveldt B *et al.* Cytosplore: Interactive Immune Cell Phenotyping for Large Single-Cell Datasets. *Computer Graphics Forum* 2016; **35**(3)**:** 171–180.

17. Godfrey DI, Uldrich AP, McCluskey J, Rossjohn J, Moody DB. The burgeoning family of unconventional T cells. *Nat Immunol* 2015; **16**(11)**:** 1114–1123.

18. Mayassi T, Barreiro LB, Rossjohn J, Jabri B. A multilayered immune system through the lens of unconventional T cells. *Nature* 2021; **595**(7868)**:** 501–510.

19. Xu B, Ji J, Ma L, Wang C, Pang L, Song Q *et al.* gammadeltaT Cells in IBD: Beneficial or Detrimental? *Immunology* 2025; **176**(3)**:** 337–348.

20. Liao CM, Zimmer MI, Wang CR. The functions of type I and type II natural killer T cells in inflammatory bowel diseases. *Inflamm Bowel Dis* 2013; **19**(6)**:** 1330–1338.

21. Haga K, Chiba A, Shibuya T, Osada T, Ishikawa D, Kodani T *et al.* MAIT cells are activated and accumulated in the inflamed mucosa of ulcerative colitis. *J Gastroenterol Hepatol* 2016; **31**(5)**:** 965–972.

22. Serriari NE, Eoche M, Lamotte L, Lion J, Fumery M, Marcelo P *et al.* Innate mucosal-associated invariant T (MAIT) cells are activated in inflammatory bowel diseases. *Clin Exp Immunol* 2014; **176**(2)**:** 266–274.

23. Tastan C, Karhan E, Zhou W, Fleming E, Voigt AY, Yao X *et al.* Tuning of human MAIT cell activation by commensal bacteria species and MR1-dependent T-cell presentation. *Mucosal Immunol* 2018; **11**(6)**:** 1591–1605.

24. Hu Y, Yang Y, Li Y, Zhang Q, Zhang W, Jia J *et al.* Th17/Treg imbalance in inflammatory

bowel disease: immunological mechanisms and microbiota-driven regulation. *Front Immunol* 2025; **16:** 1651063.

25. Ohara D, Takeuchi Y, Hirota K. Type 17 immunity: novel insights into intestinal homeostasis and autoimmune pathogenesis driven by gut-primed T cells. *Cell Mol Immunol* 2024; **21**(11)**:** 1183–1200.

26. Ouboter LF, Lindelauf C, Jiang Q, Schreurs M, Abdelaal TR, Luk SJ *et al.* Activated HLA-DR+CD38+ Effector Th1/17 Cells Distinguish Crohn's Disease-associated Perianal Fistulas from Cryptoglandular Fistulas. *Inflamm Bowel Dis* 2024; **30**(11)**:** 2146–2161.

27. Krausgruber T, Schiering C, Adelmann K, Harrison OJ, Chomka A, Pearson C *et al.* T-bet is a key modulator of IL-23-driven pathogenic CD4(+) T cell responses in the intestine. *Nat Commun* 2016; **7:** 11627.

28. Harbour SN, Maynard CL, Zindl CL, Schoeb TR, Weaver CT. Th17 cells give rise to Th1 cells that are required for the pathogenesis of colitis. *Proc Natl Acad Sci U S A* 2015; **112**(22)**:** 7061–7066.

29. Ahern PP, Schiering C, Buonocore S, McGeachy MJ, Cua DJ, Maloy KJ *et al.* Interleukin-23 drives intestinal inflammation through direct activity on T cells. *Immunity* 2010; **33**(2)**:** 279–288.

30. Feagan BG, Sandborn WJ, Gasink C, Jacobstein D, Lang Y, Friedman JR *et al.* Ustekinumab as Induction and Maintenance Therapy for Crohn's Disease. *N Engl J Med* 2016; **375**(20)**:** 1946–1960.

31. Dziegielewski C, Yuan Y, Ma C, Boland BS, Chang JT, Syal G *et al.* IL-23p19 Antagonists vs Ustekinumab for Treatment of Crohn's Disease: A Meta-Analysis of Randomized Controlled Trials. *Am J Gastroenterol* 2025; **120**(10)**:** 2260–2267.

32. Sands BE, Sandborn WJ, Panaccione R, O'Brien CD, Zhang H, Johanns J *et al.* Ustekinumab as Induction and Maintenance Therapy for Ulcerative Colitis. *N Engl J Med* 2019; **381**(13)**:** 1201–1214.

33. Rubin DT, Allegretti JR, Panés J, Shipitofsky N, Yarandi SS, Huang KG *et al.* Guselkumab in patients with moderately to severely active ulcerative colitis (QUASAR): phase 3 double-blind, randomised, placebo-controlled induction and maintenance studies. *Lancet* 2025; **405**(10472)**:** 33–49.

34. Heredia M, Barendregt DMH, Tindemans I, Klomberg RCW, Aardoom MA, Calado B *et al.* Gut-homing and intestinal TIGITnegCD38+ memory T cells acquire an IL-12-induced, ex-Th17 pathogenic phenotype in a subgroup of Crohn's disease patients with a severe disease course. *Mucosal Immunology* 2025; **18**(2)**:** 299–311.

35. Song X, Sun X, Oh SF, Wu M, Zhang Y, Zheng W *et al.* Microbial bile acid metabolites modulate gut RORgamma(+) regulatory T cell homeostasis. *Nature* 2020; **577**(7790)**:** 410–415.

36. Yang BH, Hagemann S, Mamareli P, Lauer U, Hoffmann U, Beckstette M *et al.* Foxp3(+) T cells expressing RORγt represent a stable regulatory T-cell effector lineage with enhanced suppressive capacity during intestinal inflammation. *Mucosal Immunol* 2016; **9**(2)**:** 444–457.

37. Sefik E, Geva-Zatorsky N, Oh S, Konnikova L, Zemmour D, McGuire AM *et al.* MUCOSAL IMMUNOLOGY. Individual intestinal symbionts induce a distinct population of RORγ^{+} regulatory T cells. *Science* 2015; **349**(6251)**:** 993–997.

38. Povoleri GAM, Nova-Lamperti E, Scotta C, Fanelli G, Chen YC, Becker PD *et al.* Human retinoic acid-regulated CD161(+) regulatory T cells support wound repair in intestinal mucosa. *Nat Immunol* 2018; **19**(12)**:** 1403–1414.

39. Cheng H, Nan F, Ji N, Ma X, Zhang J, Liang H *et al.* Regulatory T cell therapy promotes TGF-beta and IL-6-dependent pro-inflammatory Th17 cell generation by reducing IL-2. *Nat Commun* 2025; **16**(1)**:** 7644.

40. Kosinsky RL, Gonzalez MM, Saul D, Barros LL, Sagstetter MR, Fedyshyn Y *et al.* The FOXP3(+) Pro-Inflammatory T Cell: A Potential Therapeutic Target in Crohn's Disease. *Gastroenterology* 2024; **166**(4)**:** 631–644.e617.

41. Allegretti JR, Mitsialis V, Canavan JB, Low-Dose ILUCSG, Snapper SB. Low-Dose Interleukin 2 for the Treatment of Moderate to Severe Ulcerative Colitis. *Gastroenterology* 2023; **165**(2)**:** 492–495 e492.

42. Cui Y, David M, Bouchareychas L, Rouquier S, Sajuthi S, Ayrault M *et al.* IL23R-Specific CAR Tregs for the Treatment of Crohn's Disease. *J Crohns Colitis* 2025; **19**(3).

43. Sollid LM. Tolerance-inducing therapies in coeliac disease - mechanisms, progress and future directions. *Nat Rev Gastroenterol Hepatol* 2024; **21**(5)**:** 335–347.

44. Risnes LF, Christophersen A, Dahal-Koirala S, Neumann RS, Sandve GK, Sarna VK *et al.* Disease-driving CD4+ T cell clonotypes persist for decades in celiac disease. *J Clin Invest* 2018; **128**(6)**:** 2642–2650.

45. Hu J, Wang W, Wang M, Wu C, Jiao Y, Li Y *et al.* Immunological pathogenesis of inflammatory bowel disease: focus on tissue resident memory T cells. *Front Immunol* 2025; **16:** 1591584.

46. Bishu S, El Zaatari M, Hayashi A, Hou G, Bowers N, Kinnucan J *et al.* CD4+ Tissue-resident Memory T Cells Expand and Are a Major Source of Mucosal Tumour Necrosis Factor α in Active Crohn's Disease. *J Crohns Colitis* 2019; **13**(7)**:** 905–915.

47. Yokoi T, Murakami M, Kihara T, Seno S, Arase M, Wing JB *et al.* Identification of a unique subset of tissue-resident memory CD4(+) T cells in Crohn's disease. *Proc Natl Acad Sci U S A* 2023; **120**(1)**:** e2204269120.

48. Lockhart A, Mucida D, Bilate AM. Intraepithelial Lymphocytes of the Intestine. *Annu Rev Immunol* 2024; **42**(1)**:** 289–316.

49. Lutter L, Roosenboom B, Brand EC, Ter Linde JJ, Oldenburg B, van Lochem EG *et al.* Homeostatic Function and Inflammatory Activation of Ileal CD8(+) Tissue-Resident T Cells Is Dependent on Mucosal Location. *Cell Mol Gastroenterol Hepatol* 2021; **12**(5)**:** 1567–1581.

50. Jaeger N, Gamini R, Cella M, Schettini JL, Bugatti M, Zhao S *et al.* Single-cell analyses of Crohn's disease tissues reveal intestinal intraepithelial T cells heterogeneity and altered subset distributions. *Nat Commun* 2021; **12**(1)**:** 1921.

Figure legend

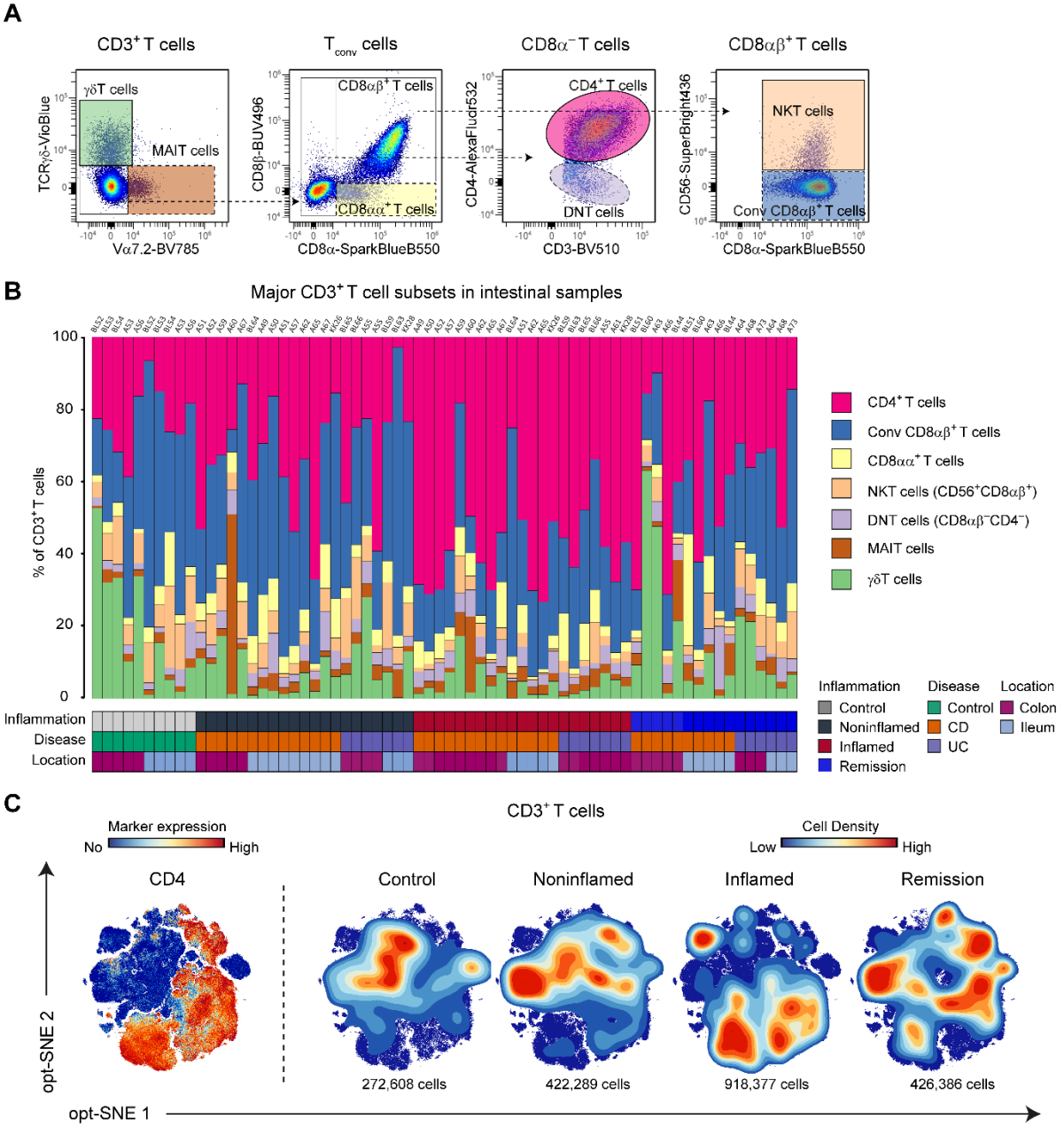

697 **Fig. 1. $CD4^+$ T cells dominate in inflamed tissue samples in IBD. (A)**, Bivariate plots showing
698 the gating strategy to identify 7 major $CD3^+$ T-cell subsets in intestinal samples, including $CD4^+$
699 T, conventional $CD8\alpha\beta^+$ T, $CD8\alpha\alpha^+$ T, NKT ($CD56^+CD8\alpha\beta^+$), Double Negative (DN, $CD8ab^-CD4^-$),
700 MAIT and γδ T cells. **(B)**, Bar graph showing cell frequencies of the 7 major $CD3^+$ T-cell subsets.
701 Depicted are the clinical metadata stratified for disease state(controls, noninflamed, inflamed,
702 remission); disease subtype (control, CD and UC); and intestinal location (colon and ileum).
703 **(C)**, opt-SNE embedding of the collective $CD3^+$ T cells derived from 68 samples plots displaying
704 CD4 expression in intestinal $CD3^+$ T cells. Density maps showing the density of cells stratified
705 for disease state. **(D)**, The frequencies of $CD4^+$ T cells stratified for disease state, disease
706 subtype and intestinal location, as percentage of total $CD3^+$ T cells. Error bars indicate the
707 median with interquartile range. *$p \leq 0.05$, **$p \leq 0.01$, ***$p \leq 0.001$, Kruskal–Wallis test with
708 Dunn's test for multiple comparisons.

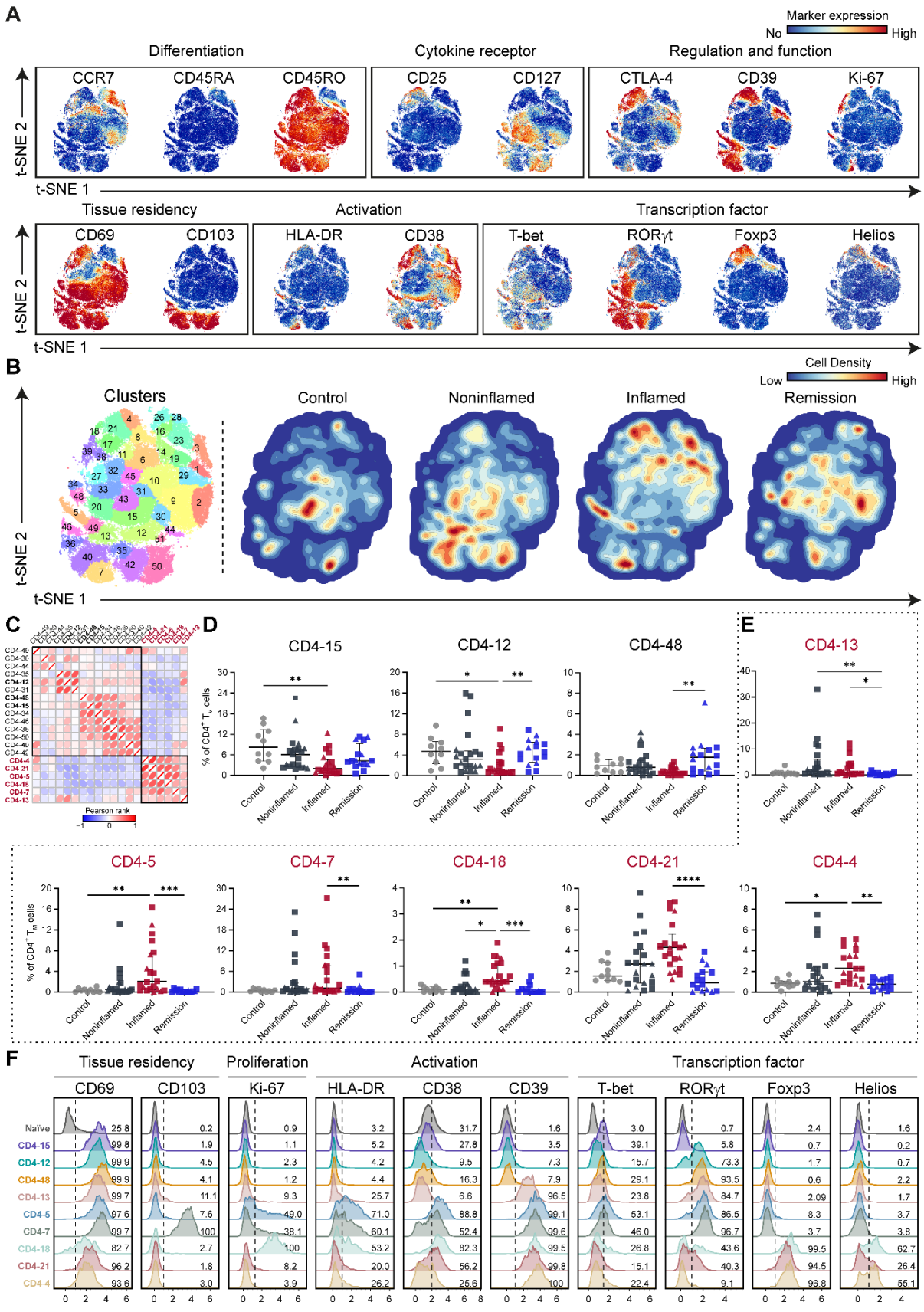

Fig. 2. The Inflammation niche harbors several activated tissue-resident CD4 T cell subsets marked by distinct transcription factor expression profiles. (A), t-SNE plots embedding of

712 65,732 intestinal $CD4^+$ memory T cells colored for the expression values of the indicated
713 markers. **(B)**, t-SNE plot showing cluster partitions and density maps showing the abundance
714 of cell subsets stratified for disease state. **(C)**, Pearson correlation matrix identifying a highly
715 correlated cluster of CD4 T cell subsets (bottom right). **(D-E)**, Dot plots showing frequencies
716 of indicated clusters stratified for disease state indicating that the CD4 T cell subsets in the
717 correlated cluster identified in C are all increased in patients samples. Error bars indicate the
718 median with interquartile range. *$p \leq 0.05$, **$p \leq 0.01$, ***$p \leq 0.001$, Kruskal–Wallis test with
719 Dunn's test for multiple comparisons. **(F)**, Overlay of histograms of $CD4^+$ naive T cells (random
720 selection of 1,000 naive cells from 68 samples) and IBD-associated clusters (derived from **Fig.**
721 **2D–E**) illustrating the expression patterns of markers related to tissue residency (CD69 and
722 CD103), cell proliferation (Ki-67), activation (HLA-DR, CD38 and CD39) and transcription
723 factors (T-bet, RORγt, Foxp3 and Helios).

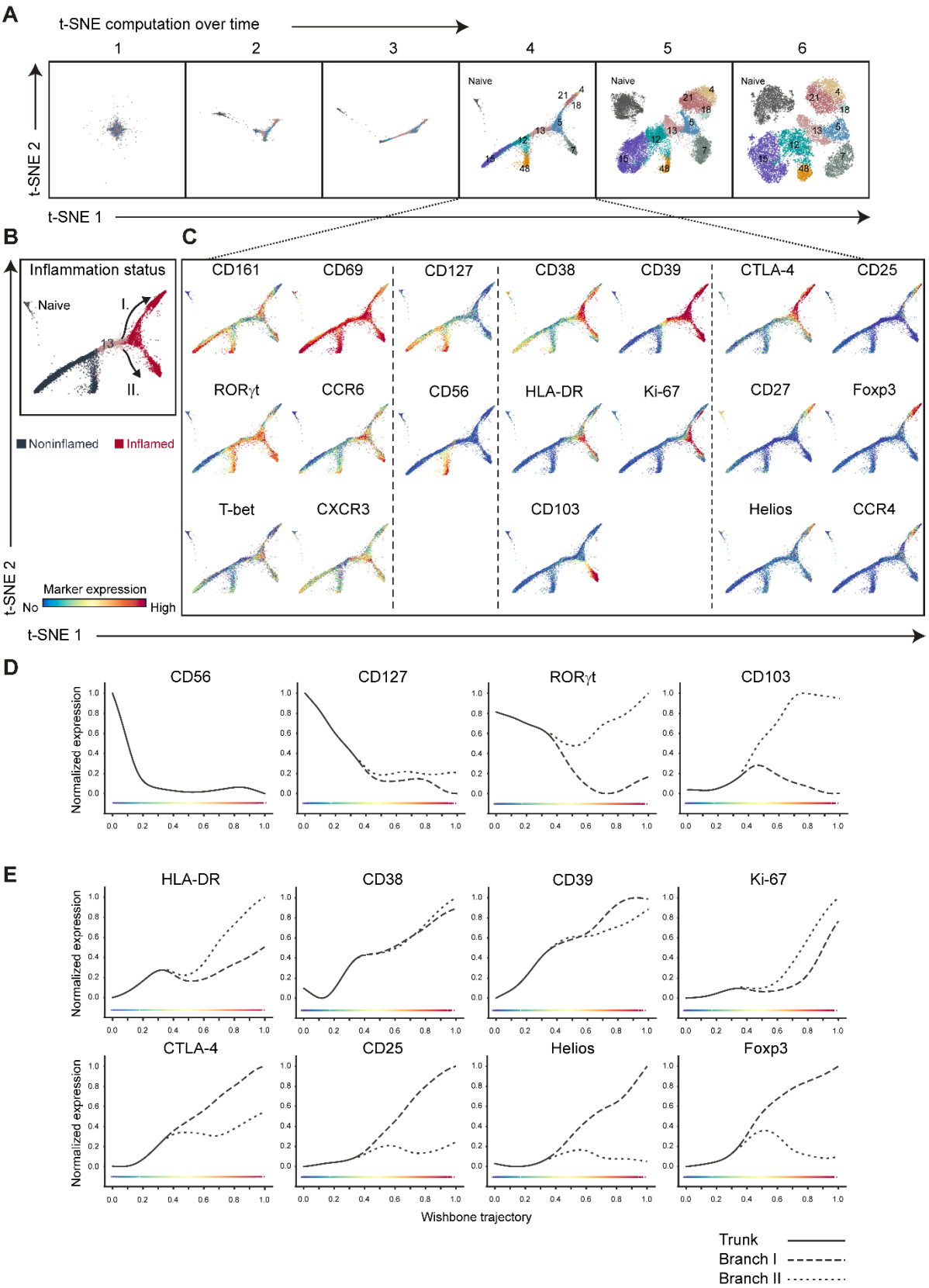

724

725 **Fig. 3. Potential differentiation trajectories of CD4 clusters during inflammation. (A)**, t-SNE

726 embeddings of CD4⁺ naive T cells (random selection of 1,000 naive cells from 68 samples) and

727 the 9 CD4 clusters derived from **Fig. 2D–F**, showing single cells at six stages over the course of
728 the t-SNE computation. Colors represent cluster partitions as described in **Fig. 2F**. **B**, stage 4
729 of the t-SNE embedding colored for inflammatory status and with arrows indicating 2
730 potential developmental trajectories associated with inflammation. **C**, Distinct marker
731 expression profiles distinguishing the non-inflamed and inflamed tissue samples. **(D–E)**, Line
732 plots generated by Wishbone (trajectory 0-1.0) showing the changes in normalized expression
733 of indicated markers along bifurcating developmental trajectories.

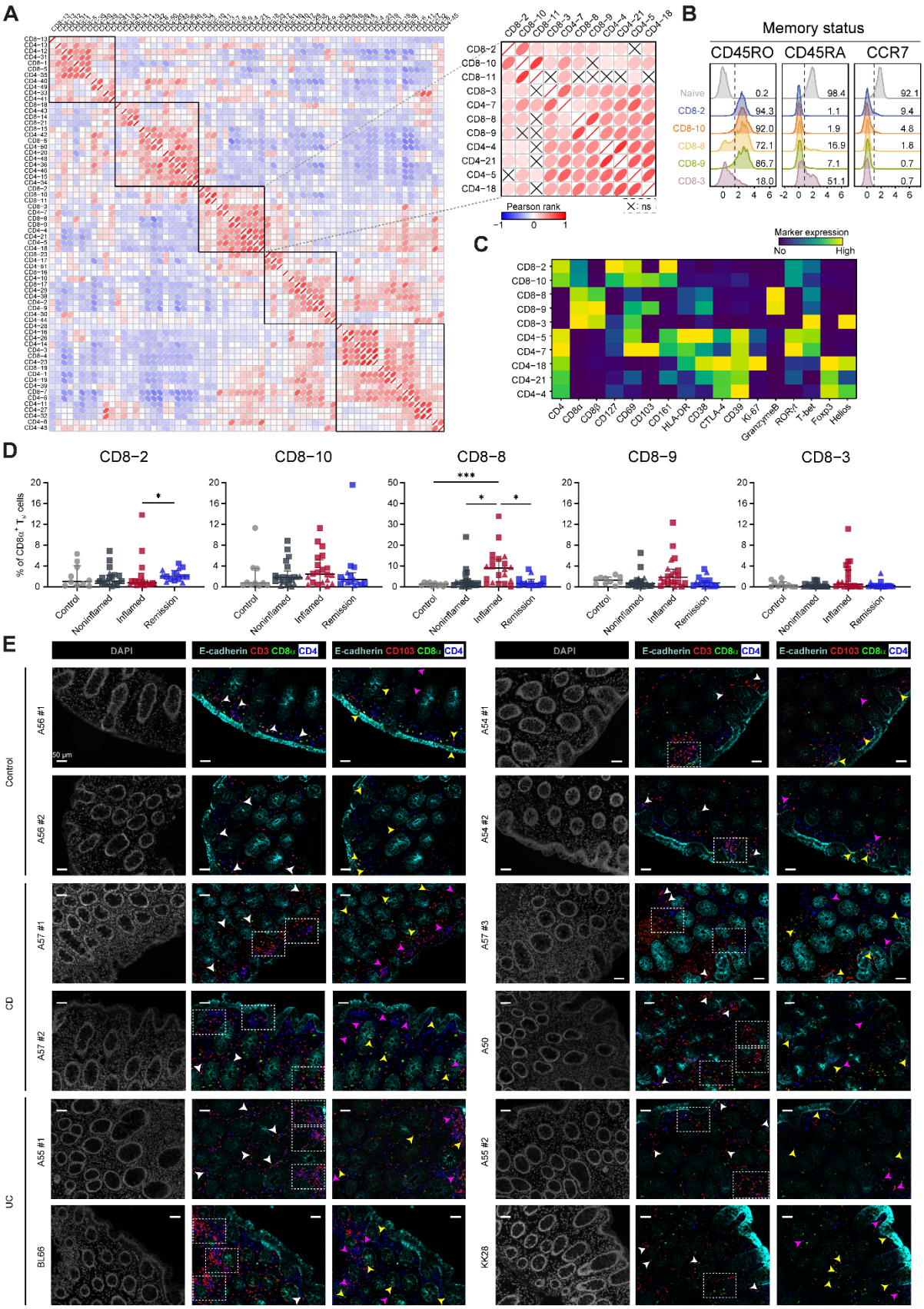

Fig. 4. CD4–CD8 T cell crosstalk in the lamina propria. (A), Pearson rank-based correlation matrix showing pairwise relationships among all memory CD4 clusters and CD8 clusters based

737 on cell percentages (of total memory $CD4^+$ and $CD8\alpha^+$ T cells) and a magnified view of the
738 third network containing the five inflammation-associated $CD4^+$ clusters together with five
739 $CD8^+$ clusters along with a statistical evaluation of inter-cluster correlations. “ns” denotes non-
740 significant correlations. **(B)**, Overlay of histograms showing the CD45RO, CD45RA and CCR7
741 expression profiles on the correlated CD8 subsets and an unrelated naïve cluster for
742 comparison. **(C)**, Heatmap showing median marker expression values of the correlated CD4
743 and CD8 clusters identified in **(A)**. **(D)**, The frequencies of CD8 clusters stratified for disease
744 state, as percentage of total $CD8\alpha^+$ T cells. Error bars indicate the median with interquartile
745 range. *$p \leq 0.05$, **$p \leq 0.01$, ***$p \leq 0.001$, Kruskal–Wallis test with Dunn’s test for multiple
746 comparisons. **(E)**, Representative images of the detection of CD103 positive $CD4^+$ and $CD8\alpha^+$
747 T cells in control, CD and UC samples, showing E-cadherin (colored in cyan), CD3 (colored in
748 red), CD8α (colored in green), CD4 (colored in blue), and DAPI (colored in grey) as nuclear
749 counterstain. Regions of CD4–CD8 cell colocalization within each ROI are marked by white
750 arrows. Yellow arrows: $CD3^+CD8\alpha^+CD103^+$ cells; magenta arrows: $CD3^+CD4^+CD103^+$ cells.
751 Scale bar, 50 µm.

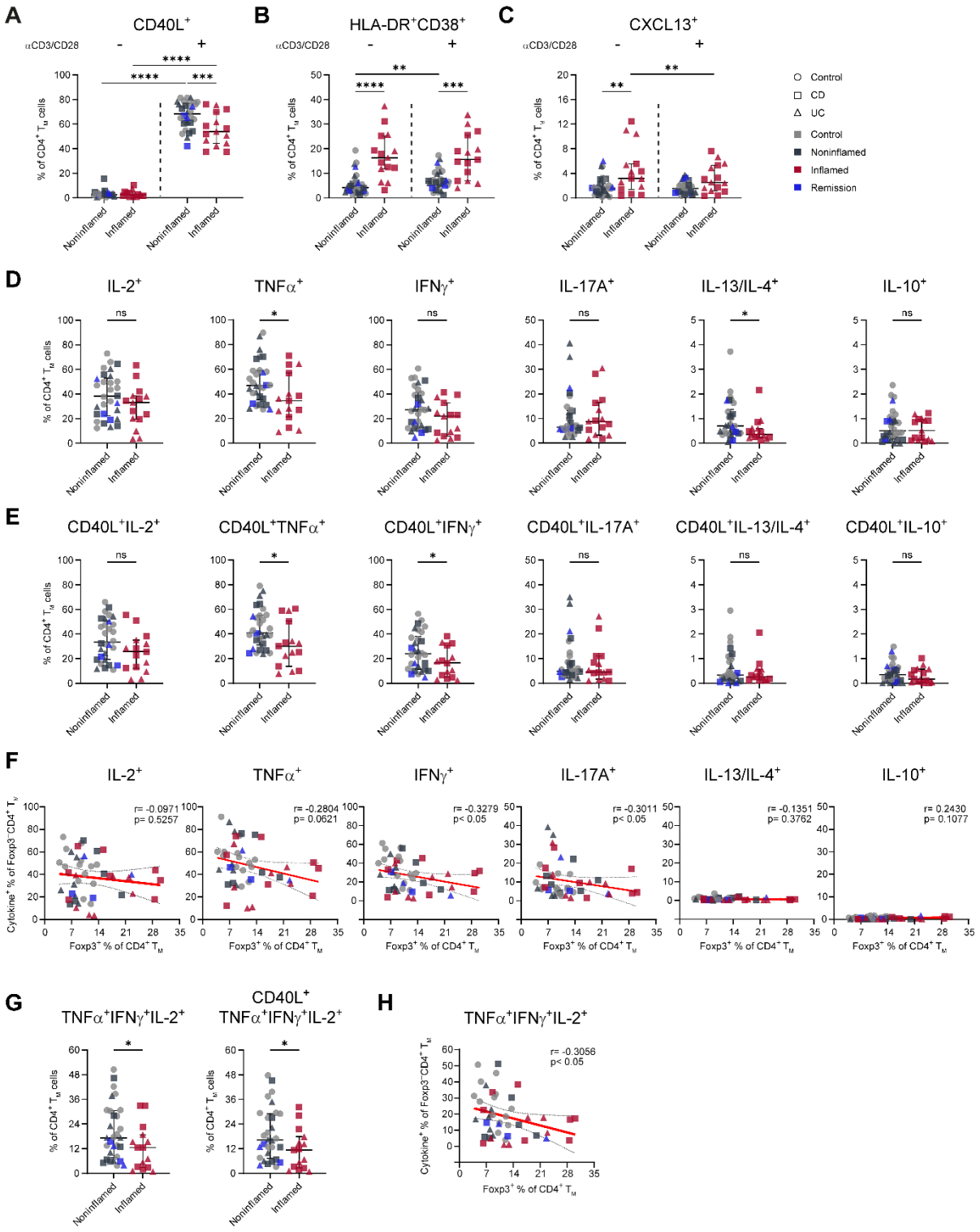

752

753 **Fig. 5. Functional profiling of intestinal CD4⁺ memory T cells.** Intestinal suspensions were

754 treated with α-CD3 and α-CD28 for 6 hours. Flow cytometry was used to quantify marker and

755 cytokine expression. **(A–C)** The frequencies of CD40L$^+$, HLA-DR$^+$CD38$^+$, and CXCL13$^+$ cells in
756 CD4$^+$ memory T cells before and after stimulation from noninflamed and inflamed samples.
757 **(D–E),** Intracellular expression of IL-2, TNFα, IFNγ, IL-17A, IL-13/IL-4 and IL-10 in total CD4$^+$
758 memory T cells **(D)** and the responsive (CD40L$^+$) memory T cells **(E)**. **(F)**, Correlations between
759 frequencies of Foxp3$^-$ CD4$^+$ memory T cells producing IL-2, TNFα, IFNγ, IL-17A, IL-13/IL-4, IL-
760 10 and frequencies of Foxp3$^+$ CD4$^+$ memory T cells were assessed using simple linear
761 regression. Spearman's rank correlation was used to determine correlation coefficients and *p*
762 values. **(G),** The frequencies of TNFα$^+$IFNγ$^+$IL-2$^+$ cells in CD4$^+$ memory T cells and the
763 responsive (CD40L$^+$) memory T cells. **(H),** Correlation analysis showing the relationship
764 between the frequencies of Foxp3$^-$ CD4$^+$ memory T cells producing TNFα, IFNγ and IL-2
765 simultaneously and Foxp3$^+$ CD4$^+$ memory T cells. Error bars indicate the median with
766 interquartile range. "ns" denotes not significant, *p≤0.05, **p≤0.01, ***p≤0.001, Mann-
767 Whitney test.

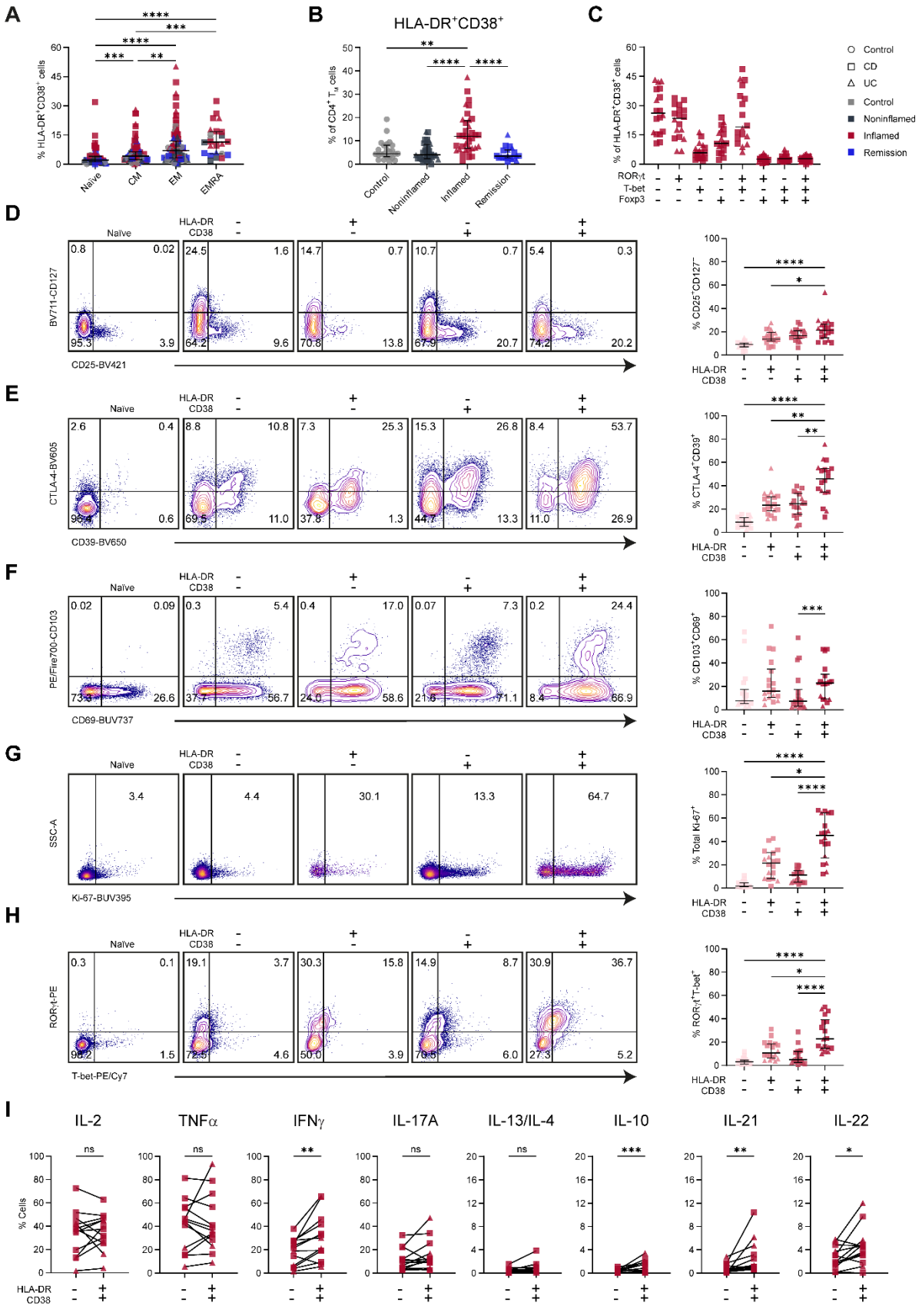

Fig. 6. Phenotypic characterization and functional profile of IBD associated HLA-DR^{+}CD38^{+} cells. (A), Dot plots showing the percentage of double positive HLA-DR and CD38 cells in the

771 naive, central memory (CM), effector memory (EM), and terminally differentiated effector
772 memory (EMRA) $CD4^+$ T cells**. (B)**, The frequencies of double positive HLA-DR and CD38 cells
773 stratified for disease state, as percentage of total $CD4^+$ memory T cells. **(C)**, Distribution of
774 cells co-expressing various combinations of the three transcription factors (RORγ, T-bet and
775 Foxp3) among HLA-DR^+ $CD38^+$ $CD4^+$ memory T cells. **(D–H)**, The frequencies of $CD25^+CD127^+$,
776 CTLA-4^+CD39^+, $CD103^+CD69^+$, Ki-67^+ and $ROR\gamma^+$T-bet^+ cells compared among four groups
777 defined by HLA-DR (positive or negative) and CD38 (positive or negative) expression, shown
778 in biaxial plots (left, naïve cells are shown for comparison) and dot plots (right) (data from one
779 representative experiment).**(I)**, Comparison of the frequencies of IL-2, TNFα, IFNγ, IL-17A, IL-
780 13/IL-4 and IL-10 positive cells in HLA-DR^-CD38^- and HLA-DR^+CD38^+ populations. Error bars
781 indicate the median with interquartile range. *$p \leq 0.05$, **$p \leq 0.01$, ***$p \leq 0.001$, "ns" denotes
782 not significant, Kruskal–Wallis test with Dunn's test for multiple comparisons or Wilcoxon tests,
783 as appropriate.

784

785